ERL2011 SUMMARIES OF WORKING GROUP 1

ERL2011 SUMMARY OF WORKING GROUP 1: PROGRESS WITH DC PHOTOEMISSION ELECTRON SOURCES

B. Dunham, et al.

ERL2011 SUMMARY OF WORKING GROUP 1: PROGRESS WITH RF INJECTORS

T. Rao, et al.

ISBN 978-3-95450-145-8

ERL2011 SUMMARY OF WORKING GROUP 1: PROGRESS WITH DC PHOTOEMISSION ELECTRON SOURCES

B. Dunham, Cornell University, Ithaca, NY 14853, USA
S. Benson, C. Hernandez-Garcia, R. Suleiman, Jefferson Lab, Newport News, VA 23606, USA
N. Nishimori, JAEA, Tokai-mura, Ibaraki 319-1195, Japan
T. Rao, Brookhaven National Lab, Upton, NY 11973, USA
M. Yamamoto, KEK Tsukuba, Ibaraki 305-0801, Japan

Abstract

This paper summarizes the recent progress made with DC photoemission electron sources for high average power Energy Recovery Linac-based light sources (ERL) and Free Electron Lasers (FEL). The progress during the past two years is discussed along with the remaining technical challenges for producing reliable, high-brightness, high average-power electron injectors.

INTRODUCTION

Much progress has been made with DC photoemission guns and their associated RF injectors since the last ERL workshop. DC photoemission guns are the best fit for machines requiring low to intermediate bunch charges (up to 100's of pC) and from low to high average currents (up to 100's of mA). RF and SRF guns, with higher cathode field gradients, are better suited for high bunch charge applications. Emittance is also a key requirement, with many ERL and FELs desiring the lowest emittance (highest brightness) possible. In this paper, we will cover the latest improvements with DC photoemission sources.

In the previous workshop [1], several alternative insulator designs were discussed to overcome the problems with commonly used cylindrical insulator stacks. A number of the choices have been built and tested, demonstrating improved performance. One system has now worked at the 500 kV level, and others are soon to follow.

Cathodes are still the most important part of a photoemission gun, DC or RF/SRF. The cathode properties determine the maximum brightness one can obtain in the final beam from the injector, and the cathode lifetime will, in part, determine the reliability and up-time for the injector. Until this year, most groups have used GaAs cathodes, as they have the lowest intrinsic emittance of any known cathode. The first emittance measurements of alkali-type photocathodes were performed recently [2, 3], demonstrating that they generate only slightly larger thermal emittance beams than GaAs at 520 nm laser wavelength. This, combined with their longer lifetime (demonstrated by several labs), makes them the cathode of choice for the time being. In the previous workshop, many load-lock systems for cathode preparation and storage were introduced. Now, load-locks are common-place for all high performance photocathode guns.

Lasers are also a critical component for photocathode guns. A number of different designs are available, depending on the frequency, wavelength and charge per bunch. A wavelength around 520 nm is often chosen for high quantum efficiency cathodes like GaAs and CsK_2Sb. The frequency can vary greatly, from tens of MHz to 1300 MHz. Lower frequency lasers are often commercially available, while higher frequency systems are usually custom built.

As more DC photoemission guns with RF/SRF accelerating modules come on-line, operational issues are becoming of more interest to the DC gun community. How to deal with very high average power beams is still not well understood. Issues like beam halo, large dynamic range diagnostics, machine protection, beam dumps, and radiation safety become more important as we construct electron injectors in the 500 kW to 1 MW range.

This summary paper will cover the advances in each of these areas since the last ERL workshop in 2009.

PHOTOCATHODES

Bruce Dunham

Cathodes are clearly the most important component of any photoemission gun, whether it is DC, RF or an SRF type. A number of recent photocathode workshops have been very well attended (https://indico.bnl.gov/conferenceDisplay.py?confId=290, http://photocathodes2011.eurofel.eu/). Much of the current knowledge is summarized in the review paper by Dowell [4].

For the high brightness, high-average current applications for ERLs and FELs, only semiconductor-type cathodes are considered, as the low quantum efficiency (QE) of metal cathodes precludes their use. There are several key parameters that a cathode must have for these high performance injectors. The first parameter for a cathode is high QE (5-10%) at an easily obtainable laser wavelength (520 nm, for instance) in order to reach 100's of mA average current. Second, a low thermal emittance is required (the lower the better) to generate bright beams. Early simulations showed that it is possible to nearly recover the cathode thermal emittance after accelerating the beam to 5-10 MeV [5], and these simulations have recently been verified experimentally [6]. Third, a very fast (sub-ps) electron response time is an integral part of reaching small emittances. Long tails lead to emittance growth, and limit the effectiveness of laser pulse shaping. Finally, the cathode must last a relatively long time while delivering

ISBN 978-3-95450-145-8

the desired beam current under operational conditions. Without this, one cannot build a reliable injector with good up-time.

GaAs and GaAs-like materials have been used as sources of polarized electrons for many years. GaAs has also been used for non-polarized applications, such as DC guns (at the Jlab FEL [7], for example). GaAs has a number of properties that make it attractive for non-polarized beams, but also has several that make its use difficult.

Obtaining high QE of 10-20% for GaAs is relatively straightforward for green laser wavelengths, making it a good candidate for obtaining high average currents with modest laser power. The QE falls off quickly for longer wavelengths. The response time for GaAs is quite fast (sub-ps) for green and shorter wavelengths [8] as long as the QE is below ~10%, but becomes much longer as the wavelength approaches the bandgap energy. GaAs also has the smallest measured intrinsic emittance of any know cathode [9], but this occurs at wavelengths approaching the bandgap where the QE becomes small. Thus, it is not possible to use GaAs to simultaneously get high QE, fast response time, and ultra-low intrinsic emittance. Finally, because the GaAs photoemission process is a surface phenomenon, extreme ultra-high vacuum is required, making it very sensitive to any vacuum excursions during operation. Continued R&D into GaAs-like materials will be very important for the future, in order to find a cathode with all of the key parameters needed for high-brightness, high average power injectors. It is important to note, that even with these difficulties, currents as high as 25 mA at 5 MeV have been produced using GaAs [6].

In the 1990's, alkali photocathodes were used in several photoemission guns as they were much more robust in terms of vacuum requirements. A CsK_2Sb cathode was used to produce the highest average current beam to date [10]. They were not considered as candidates for high-brightness sources until recently, due to the assumption that the intrinsic emittance would not be as low as GaAs. Recent measurements [2, 3, 11] have dispelled that myth, demonstrating that alkali cathodes produce electrons with only a slightly higher transverse thermal energy than for GaAs around 520 nm. Much of the confusion in the past resulted from the misconception that GaAs could produce thermal or sub-thermal transverse energy electron beams at useful laser wavelengths. As discussed above, these sub-thermal beams are only generated using near band-gap radiation where the QE is low and the response time is slow, which is not compatible with high-power, high-brightness injectors. Using very thin GaAs samples can mitigate the problem with slow response time.

Due to these new measurements, a number of groups have switched to using alkali photocathodes for beam operations instead of GaAs. In addition, several groups have demonstrated long-term, stable cathode operation at 20 mA average currents (both DC beam at low energy (200 keV) [12], and CW beams at high energy (5 MeV) [13]). QE values of 5-10% are readily achieved, and the response time is quite fast (<1 ps). There is still plenty of work to do to determine the optimum growth recipes, best substrate to use, and damage mechanisms during extended operations. The vacuum requirements are not as stringent as for GaAs, somewhat simplifying the design of load-locks and gun vacuum systems.

Having a robust cathode to use for commissioning high power injectors will free up cathode designers to concentrate on finding the ideal cathode for future light sources. Other possibilities include: engineered materials, like was done for polarized electron sources; GaN-like materials [14]; and improving the theoretical understanding of photoemission for NEA and PEA materials.

HIGH VOLTAGE INSULATORS

Nobuyuki Nishimori and Riad Suleiman

Operation of DC photoemission guns at 500 kV or more has been a technological challenge to be faced since the first ERL workshop in 2005 [15]. The highest operational voltage has however stayed at 350 kV. The most serious problem is field emission from a cathode support electrode, which can lead to voltage breakdown, insulator punch-through and other problems on the ceramics. In order to solve this field emission problem, a segmented insulator, an inverted insulator and an insulator with a controlled bulk resistivity were proposed at the last ERL workshop in 2009 [1]. In this section, the progress of the segmented and inverted insulator developments over the past two years is summarized.

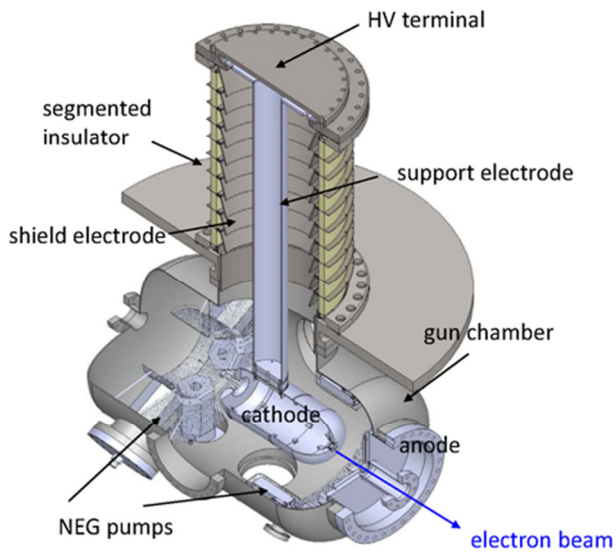

Figure 1: A DC photoemission gun with a segmented insulator at JAEA.

Segmented Insulators

A segmented insulator has been widely used for DC electrostatic accelerators. The insulator consists of ceramics and metal rings alternatively stacked in series

ISBN 978-3-95450-145-8

Table 1: Parameters of Segmented Insulators for DC Photoemission Guns

Institute	HV(kV)	Segments	Ceramics	Support electrode	Shield electrode	Multiple insulators	Ref.
JAEA (existing)	500	10	99.8%Al_2O_3 A99P 400 mm diameter 750 mm in height Rings are 65mm high x 20mm thick Ceramic by Shinagawa Fine ceramics Brazed by Hitachi Haramachi	Titanium 101.6 mm diameter	Titanium 290mm inner diameter	Single	[21]
Cornell (existing)	750	14	99.8% Al_2O_3 Rings are 50mm high x 20mm thick Height: 448mm x 2 Ceramic by Friatec Brazed by Friatec	Stainless Steel 110 mm diameter	Copper, 363 mm inner diameter	Two	[22]
KEK (existing)	500	10	Al_2O_3 based ceramic (TA010) 400mm diameter Height:398mmx2 Rings are 65mm high x 20mm thick Ceramic by Kyocera Brazed by Kyocera	Titanium 101.6 mm diameter	Titanium 290 mm inner diameter	Two	[23]
IHEP (planned)	500	10	Al_2O_3 (Kyocera/CPI/other company) Detailed design is in progress	Titanium Detailed design is in progress	Titanium Detailed design is in progress	Two	[24]

(see Figure 1). This structure provides means to connect an additional electrode to the metal ring, which can shield ceramic surfaces from field emission cathode support electrode. The field emission current is drawn to ground through an external resister connected between adjacent electrodes. These segmented insulators have been used for the 100 kV gun at NIKHEF [16], the 200 kV gun at Nagoya University [17] and the 230 kV gun at JAERI FEL [18]. The use of segmented ceramics for a 500 kV photoemission gun was proposed at JAEA and KEK in 2008 [19].

One of important parameters for the design of a segmented insulator is the surface electric field of a cathode support electrode, since the field emission generated from the support electrode may damage the ceramics. The surface field on the support electrode is roughly given by

$$E_r = \frac{V}{r \ln(R/r)},$$

where V is the potential difference between the support electrode with outer radius r and the additional shield electrode with inner radius R. Substitution of JAEA gun parameters r=50.8 mm and R=145 mm yields E_r=9.38 MVm^{-1} for V=500 kV. The surface electric field anywhere on the electrodes should be smaller than the voltage breakdown criteria. The breakdown criteria for large area electrodes decrease with increasing voltage due to total voltage effect. The criteria for V=500 kV is about 10 MVm^{-1} [1, 20].

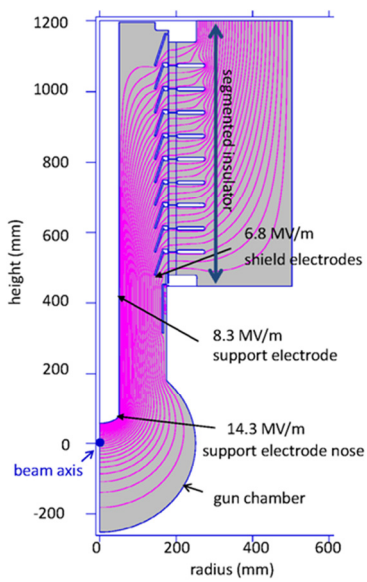

Figure 2: Static electric field calculation of segmented insulator with a support electrode and gun chamber at JAEA. The high voltage is 500kV.

The field emission from shield electrodes to the ceramic segments also needs to be avoided. This electrode is a cathode for the ceramic surface and an anode for the support electrode. The maximum field emission energy to the ceramic is equal to the total applied voltage divided by the number of segments. For a gun with ten segmented ceramics, the field emission energy is 50 keV for V= 500 kV. Since the voltage breakdown criteria at 50 kV is much higher than that at 500 kV, the damage on the ceramics caused by the field emission from shield electrodes will be small. Increasing

ISBN 978-3-95450-145-8

of the number of segments also helps to provide uniform electric field on the ceramic surface.

Figure 2 shows an example of the static electric field calculation for the segmented insulator at JAEA. The maximum electric field on the support and shield electrodes are 8.3 MVm^{-1} and 6.8 MVm^{-1}, respectively, which are smaller than the voltage breakdown criteria at 500 kV. The outer radius of the ceramics is determined to be 200 mm. Similar guns with segmented insulators have been developed in Cornell and KEK. Parameters of segmented insulators for DC photoemission guns under development or planned are listed in Table 1.

Multiple insulator stacks have been employed at Cornell and KEK. This helps to simplify installing shield electrodes inside the insulators and to avoid complete replacement of the insulators in case of failure of a single stack.

A segmented insulator was also used for the 1 MV bushing of the international thermonuclear experimental reactor (ITER) neutral beam injector (NBI) [25, 26, 27]. A negative deuteron ion beam of 40 A with duration of 3600 seconds at 1 MeV is required. The electrical bus bars and water cooling lines necessary for the negative ion source placed at -1.0 MV terminals are provided through the 1.0 MV bushing. The bushing therefore has a center conductor at -1.0 MV as an electrostatic shield. The structure is very similar to Fig. 1. High voltage conditioning up to 973 kV was demonstrated at Cadarache in France, when $2x10^{-2}$ Pa of hydrogen or helium gas was added in the high voltage chamber [26]. This additional gas is found to be very effective for high voltage conditioning.

Inverted Insulators

The Jefferson Lab photocathode gun employs inverted insulator geometry [28] where a ceramic insulator extends into the vacuum chamber, as shown in Figure 3. The primary benefit of this approach is that a large metal structure is not required to support the cathode electrode. As a result, there is significantly less surface area biased at high voltage, and consequently there is less metal to generate electrons. The design also creates electrostatic field lines that tend to deliver field emitted electrons toward the grounded vacuum chamber, rather than to the insulator where damage can occur. Another appealing feature is that the insulator is a common element of medical x-ray sources, and therefore relatively inexpensive compared to cylindrical insulators purchased solely for accelerator electron gun applications. Finally, because there is no exposed high voltage, corona shields and a tank for dry nitrogen gas or SF_6 are not required.

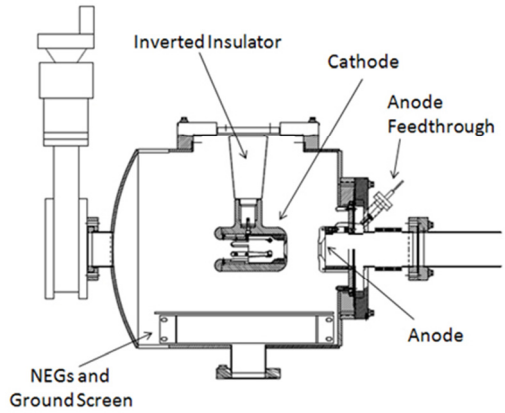

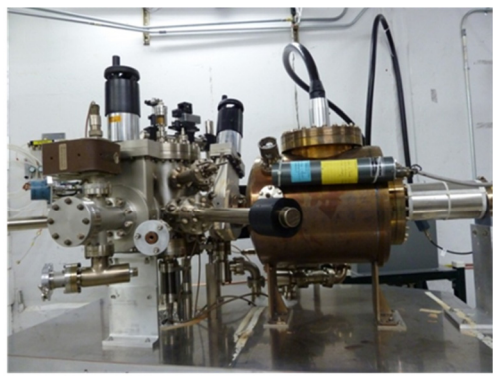

Figure 3: (Top) Cross section of the Jefferson Lab inverted gun HV chamber. (Bottom) The anode is electrically isolated and connected to a pico-ammeter to detect field emission. Commercial R28 HV cables connect the 225 kV Spellman HV supply to the gun through an oil tank. The oil tank allows for 100 MΩ resistor to be connected in series during HV conditioning the gun. An x-ray radiation detector is mounted on the side of the gun HV chamber.

Two guns have been built at Jefferson Lab based on the compact inverted insulator design [29]. One gun provides the polarized electron beam at the Continuous Electron Beam Accelerator Facility (CEBAF) and the other is used for more aggressive tests at a dedicated test facility. Both guns employ tee-shaped cathode electrodes. The CEBAF cathode electrode is made of 316L stainless steel polished to sub-micron finish using diamond grit. It was high voltage processed to 150 kV without field emission and now provides beam at 130 kV. The second gun uses a cathode electrode made of large-grain niobium and was successfully conditioned to 225 kV (the maximum voltage of the supply) without field emission. Efforts to build a 350 kV inverted gun using commercial R30 HV cables and connectors are underway. Simultaneously, we are working on a 500 kV inverted gun in collaboration with Jefferson Lab FEL. For this gun, commercial connectors are not available, so we are engineering appropriate HV connections, and considering means to allow for photocathode cooling.

ISBN 978-3-95450-145-8

HIGH VOLTAGE CONDITIONING TECHNIQUES

Carlos Hernandez-Garcia, Nobuyuki Nishimori and Riad Suleiman

Electrodes in DC photoemission guns must be high voltage conditioned prior to normal operations at the desired voltage for reliability without field emission. Typically DC guns are conditioned 10% to 25% higher than the operational voltage to remove electron emission sites in a controlled manner. When precautions are taken towards producing smooth electrode surfaces and extreme high vacuum procedures implemented for cleaning and assembly, activity is not observed below 250 kV [30, 21]. Beyond this voltage, conditioning is usually performed at about 5-10 kV per hour to maintain the overall vacuum level below $5x10^{-6}$ Pa. This is typical for semiconductor photoemission guns where ultra-high vacuum conditions are necessary for good cathode lifetime, for other types of guns higher values may be acceptable. The high voltage power supply current is limited to a few μA above background to minimize damage to the electrode and/or to the current limiting resistor. Above 300 kV, voltage induced gas desorption slows down conditioning [1]. For example, in the JLAB FEL DC photoemission gun, it takes one hour for the vacuum to recover after each 1 kV increment, while the JAEA DC photoemission gun has been conditioned at a rate of 4 kV/hr.

It has also been observed that the higher the voltage, the longer it takes for the vacuum level to recover, assuming the incremental voltage steps are the same value [1]. In some instances the voltage is lowered to maintain the emission current at a few μA above the power supply's background for preventing damage, but at the same time the excess current needs to be sufficiently high to induce melting of the emitter by Joule heating. Often times this requires increasing the voltage beyond the last set point at which voltage induced gas desorption was last observed, therefore coupling field emission processing with voltage induced gas desorption processing.

Two results are noteworthy since the last ERL Workshop in 2009 [1]. The JAEA DC photoemission gun, built with a segmented insulator, has been conditioned to 550kV, and the CEBAF polarized source group has characterized various types of niobium electrodes in a high voltage test stand. In addition to those results, both the Cornell and the JLab FEL DC photoemission guns were rebuilt with cylindrical insulators of a new material (AL-970CD) from Morgan Advanced Ceramics that promised charge dissipation through some degree of conductivity embedded in the bulk. Unfortunately the new insulators in both the Cornell and the JLab FEL DC guns suffered punctures at ~450 kV [30]. The leaks were sealed but re-processing was limited to ~400 kV. The Cornell gun has been operating since then at 350 kV. Despite 100 hours of conditioning with Krypton gas, the JLab FEL gun has been operating at 325 kV [31]. Re-processing of both electron guns was limited by re-opening of the initial punch-through leak. The most likely mechanism is that field emitted electrons from the stem electrode, which is coaxial to the cylindrical insulator, accumulate charge in the bulk of the insulator. As the charge did not dissipate as advertised, the accumulated charge was high enough to violently discharge to ground, effectively vaporizing the material and causing micro holes, which after many events connect the vacuum side of the insulator to its outer surface letting SF_6 into the vacuum environment.

JAEA DC Gun 550kV Conditioning

The segmented insulator with a support electrode at JAEA was successfully high voltage processed up to 550 kV in 2009 [21]. In order to study the field emission effect from the support electrode, the cathode and anode electrodes and NEG pumps were not installed in the gun chamber initially. The ceramics and high voltage chamber were baked at 190 degree for eight hours prior to the processing. A 1000 Ls^{-1} turbo molecular pump was used in this test and the base pressure was $2x10^{-8}$ Pa. Figure 4 shows the high voltage test results. The voltage started at 250 kV, and then took 15 minutes for each 1 kV step up to 500 kV. The processing speed becomes slower above 500 kV because of increased radiation.

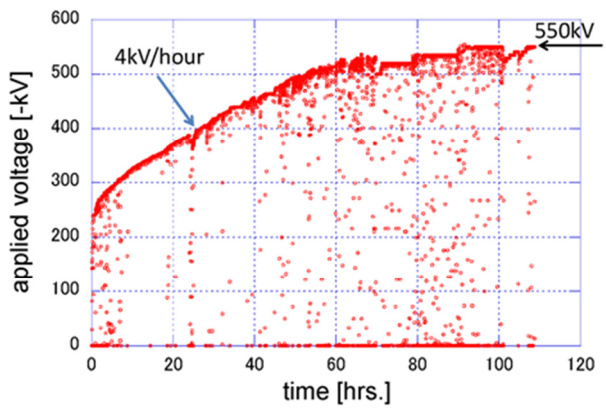

Figure 4: High voltage processing of a segmented insulator with a support electrode at JAEA [21].

Stable operation of the segmented insulator over eight hours was also demonstrated for the prospect of future light source applications, as shown in Figure 5. The top figure shows high voltage versus current as a function of time. The bottom shows radiation and vacuum pressure as a function of time. No indication of discharge or local heating due to dark current was observed. Thus 500 kV was applied between high voltage and ground terminals of the insulator. It is concluded that the segmented insulator with shield electrodes can solve the field emission problem from a support electrode at voltages up to at least 500 kV.

ISBN 978-3-95450-145-8

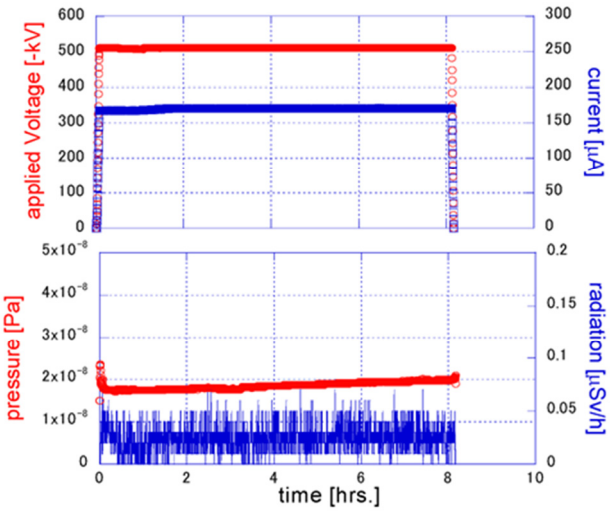

Figure 5: A long-time holding test for eight hours at JAEA [20]. The top figure shows applied voltage (red) and current of HV power supply (blue) as a function of time. The bottom figure shows pressure (red) and radiation (blue).

The next step was to repeat the same HV processing with electrodes and NEG pumps in place for beam generation. The cathode electrode should be designed for its maximum surface electric field to be less than voltage breakdown criteria at 500 kV. The maximum electric field of cathode electrode and field on the cathode center are 10.3 MVm^{-1} and 6.7 MVm^{-1}, respectively, at JAEA. The gap between cathode and anode electrodes is 100 mm. High voltage processing up to 526 kV was demonstrated in 2011 at JAEA [32].

The conditioning of the support electrode (without the cathode electrode) and the segmented insulator was mostly done manually. At voltages higher than 300 kV and when the HVPS tripped on vacuum or radiation, a few minutes of waiting time allowed the vacuum to recover before ramping up to the voltage set-point with a computer program. It takes another a few minutes to ramp back to the voltage set-point. Then the voltage was increased manually in 0.3 kV steps while monitoring vacuum, radiation, voltage and current. Once the vacuum and radiation exceeded their limit point, the HVPS was shut off by the computer program. The interlock limits were set to $5x10^{-6}$ Pa for vacuum and to $3x10^{-6}$ Svh^{-1} with radiation monitors placed 50 cm from the vacuum chamber. The average current was limited to 1 μA by the constant current circuit shown in Figure 6. If the average discharge current exceeds 1 μA, the HVPS cannot maintain Constant Voltage mode and the voltage drops quickly. The voltage drop helps to reduce field emission current. Then the voltage recovers gradually as the power supply charges its capacitor back. Finally the operational mode returns to Constant Voltage mode. The time spent at voltage during processing from 250 kV to 550 kV was about 100 hours. Considering the vacuum recovery time it took a total of four weeks. There was no inert gas processing in the conditioning of the JAEA gun.

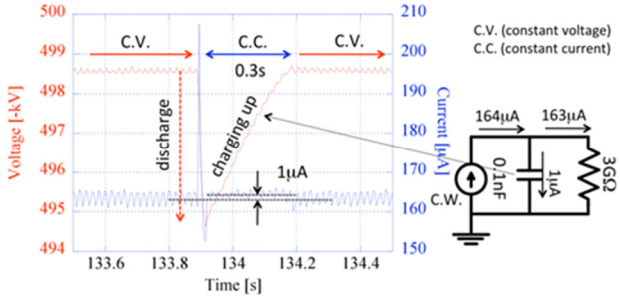

Figure 6: The circuit used in conjunction with the Cockcroft-Walton generator for high voltage processing in the JAEA gun.

When the cathode electrode was mounted to the support electrode (Figure 1) field emission made processing more difficult. Usually the conditioning of electrodes in DC photoemission guns is performed under ultra-high vacuum conditions achieved after thorough vacuum bakeout of the system at 125-250º C. This process nominally renders hydrogen dominated environment in the range of $6x10^{-8}$ Pa to $6x10^{-9}$ Pa. However, high voltage processing can be done without those stringent vacuum conditions. Once it was realized that electron emission was triggered by particulates falling from the NEG cartridges onto the cathode electrode, the gun was vented with dry nitrogen, the electrodes wiped off with lint-free tissue, and then the gun vacuum chamber evacuated without baking to $3x10^{-9}$ Pa with NEG re-activation. High voltage processing continued until it was stopped again by falling NEG particulates. The cleaning process might be repeated, but the gun vacuum chamber was exposed to air for examination of NEG cartridges for source of falling particulates.

Niobium Electrodes

Niobium is used to make superconducting RF cavities and there are many reports of field-emission free operation at field gradients exceeding 30 MVm^{-1}. Although these results were obtained at 2 K and with RF electric fields, it seemed reasonable to evaluate niobium in a DC photocathode gun at room temperature [33]. An appealing feature of niobium is that the cleaning procedures for producing good HV surfaces are well known from the SRF community. The niobium electrode was chemically etched in a mixture of hydrofluoric (49%), nitric (69%) and phosphoric (85%) acid with mixing ratio 1:1:1 at room temperature. This technique is referred to as buffered-chemical polishing (BCP). Besides taking advantage of BCP, other SRF techniques were adopted including high pressure rinsing with ultra-pure de-ionized water and 900°C vacuum degassing [34].

The first application of high voltage on the second inverted gun was disappointing, with field emission detected at voltage >140 kV. By increasing the applied voltage, some field emitters were eliminated (Figure 7

ISBN 978-3-95450-145-8

(top), blue data points) but conditioning was limited to 225 kV. Figure 7 (bottom) shows the x-ray radiation measured during HV conditioning. Not surprisingly, photocathode lifetime was poor while delivering beam at 200 kV due to low level field emission which served to degrade the vacuum within the gun.

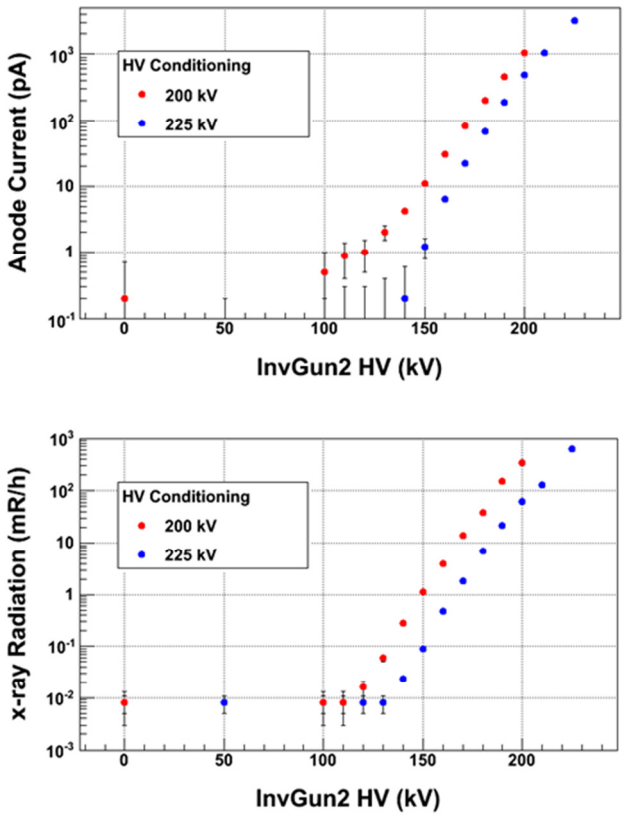

Figure 7: (Top) Field emission measurements during the initial HV conditioning of the second inverted gun. Going to higher voltage served to eliminate some field emitters (blue data points). (Bottom) The x-ray radiation measurements performed during HV conditioning.

The large-grain niobium electrode was removed from the gun and inspected, whereupon the surface finish was deemed too rough. Another BCP treatment was performed resulting in a cumulative removal of about 100 μm of surface material (surface roughness < 0.5 μm). Upon re-installation of the cathode electrode into the gun and vacuum chamber bake-out, no field emission was detected at voltage up to 225 kV, see Figure 8. Similarly, no x-rays were detected and there was no vacuum activity in the gun chamber.

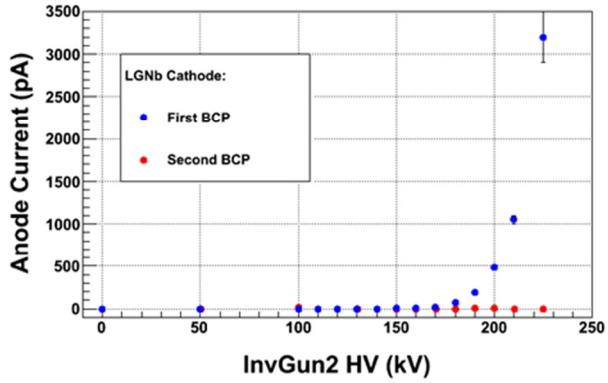

Figure 8: Field emission measurements during HV conditioning. A second BCP treatment successfully eliminated field emission to 225 kV.

VACUUM TECHNIQUES

M. Yamamoto

A high brightness electron gun which utilizes a gallium arsenide (GaAs) photocathode requires an extreme high vacuum (XHV) condition to preserve a negative electron affinity state for a sufficiently long time under high current operation.

The ultimate pressure P is given by $P=Q/S$, where Q is a total outgassing rate of the system and S is the effective pumping speed. Therefore, all of the vacuum components in the gun system should have a low outgassing rate, and the pumps should function under XHV. The outgassing rate and the pumping speed of the actual gun vacuum system are important parameters to realize XHV condition.

At KEK, a 500 kV DC-gun was constructed with a segmented insulator as shown in Figure 9. The gun consists of a titanium chamber, a pair of segmented insulators and titanium guard ring electrodes, with surface areas of 2.39 m^2, 1.26 m^2 and 2.02 m^2, respectively. The total volume of the system is 0.333 m^3.

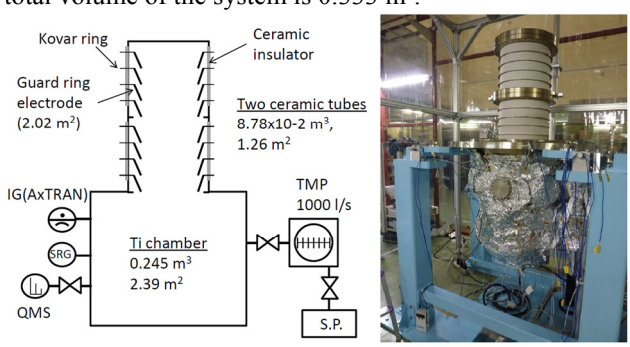

Figure 9: Schematic diagram of a KEK 500 kV DC gun vacuum system and its photograph.

ISBN 978-3-95450-145-8

The system was baked ~200C for 100 hours before the outgassing rate measurement. The total outgassing measurement was obtained with the rate-of-rise (RoR) method using a spinning rotor gauge (SRG). The ultimate pressure of the system reached 7.2x10^{-9} Pa (equivalent for nitrogen) after the bake-out process. The total outgassing rate of the system was estimated to be 1.05x10^{-10} Pa·m^{3}s^{-1} equivalent for hydrogen as shown in Figure 10 [35].

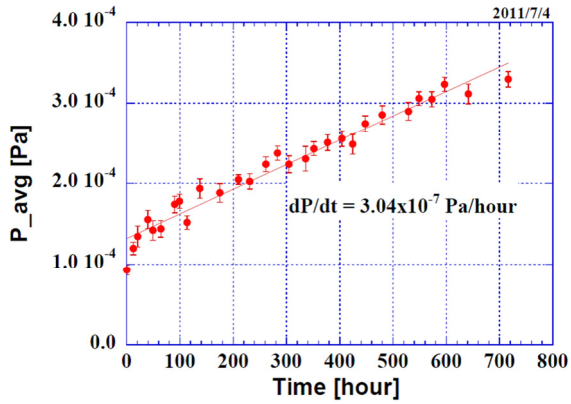

Figure 10: Result of the RoR measurement by the SRG for about 1 month. The value of pressure is equivalent for nitrogen.

At KEK, we demonstrated measurement of pumping speed of a bakeable cryopump, in which the G-M refrigerator is separated spatially from cryopump housing in order to bakeout the pump including cryopanels and adsorbent [36]. Such pumps have been reported to produce XHV conditions, without the usual arrays of NEG pumps. The apparatus is shown in Figure 11.

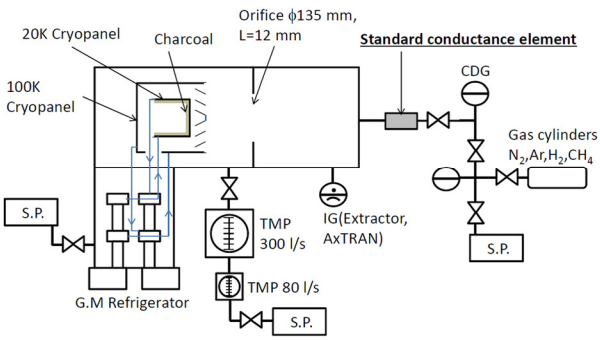

Figure 11: A 20 K bakeable cryopump and a pump speed measurement system with a precise gas flow control system using a standard conductance element.

One of the key issues for measuring pumping speed is to accurately control the gas flow to the test chamber. In this experiment, we use a standard conductance element [37]. The gas flow Q [Pa·m^{3}s^{-1}] through the standard conductance element is estimated as

$$Q\,[\mathrm{m^3/s}] = P_f\,[\mathrm{Pa}]\cdot C\,[\mathrm{m^3/s}]\sqrt{\frac{28}{M_a}}\sqrt{\frac{T\,[\mathrm{K}]}{T_0}}$$

where P_f is the pressure in the inlet of the element measured by a capacitance diaphragm gauge (CDG), M_a is the molecular mass of gas, T is the temperature of the element, C [m^3/s] is the experimentally determined conductance of the element for nitrogen at the temperature T_0. A conductance of 3.01x10^{-10} Pa m^{3}s^{-1} at the temperature of 300 K was used for the standard element.

The result of the effective pumping speed measurement of the 20 K bakeable cryopump is shown in Figure 12 [34]. The pumping speed was obtained for nitrogen, argon, methane, and hydrogen. The ultimate pressure was limited to 1x10^{-9} Pa by adsorption equilibrium of hydrogen in this experiment.

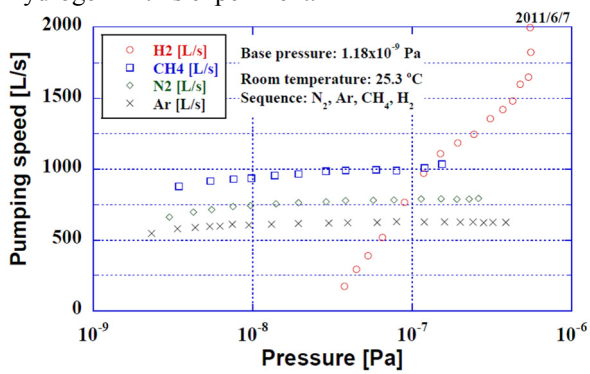

Figure 12: Result of the pumping speed of the 20 K bakeable cryopump for hydrogen, methane, nitrogen and argon.

LASER SYSTEMS

Triveni Rao and Bruce Dunham

The parameters of the laser system driving photoinjectors are determined by the cathode's characteristics as well as those of the electron beam for the intended application, and hence, cover a wide range. Typically, for high current injectors, high QE cathodes irradiated with ~2 eV photons are preferred, since laser systems meeting most of the specifications are available commercially. Until recently, most high current injectors relied on diode pumped solid state (DPSS) lasers. Lately, there has been sufficient progress with fiber lasers that they present a viable alternative to the DPSS laser systems. In the following sections, we will discuss the performance characteristics of both these devices.

Both these lasers have the same architecture: i) an oscillator (or an oscillator and modulator combination) that sets the operating wavelength, pulse duration, repetition rate, and timing stability, ii) an amplifier that maintains all the above parameters but increases the energy/pulse of the output beam, and iii) a non-linear medium that converts the ~1 eV photons from the amplifier to ~2 eV or ~3 eV photons. A second modulator can be introduced between the amplifier and the nonlinear medium to accommodate the required pulse structure, while maintaining a constant thermal load on the

ISBN 978-3-95450-145-8

oscillator and amplifier, thereby, preserving the stability of laser output.

An example of a DPSS laser is the system for the BNL ERL program. It is designed to deliver up to 5 W at 355 nm, with pulse duration of ~10 ps, repetition rate of 9.38 MHz, synchronized to an external 703.5 MHz master clock with a sub-picosecond jitter. A pulse selection system is incorporated to allow the ramp up from a single pulse to a series of micro pulses in a macro pulse with variable repetition rate (up to 10 kHz), and ultimately, to a continuous 10 MHz to facilitate the recovery of electron energy in the linac.

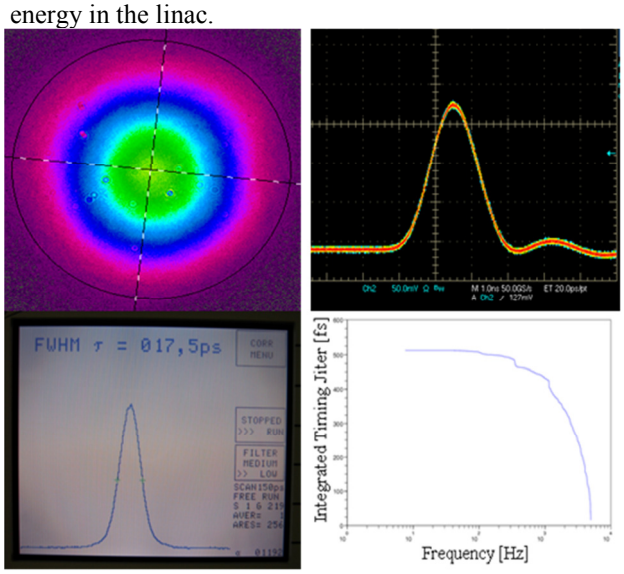

Figure 13: (clockwise from upper left) Transverse profile of the amplified beam; IR energy stability, contrast is better than 1:1800; pulse duration of the IR beam; jitter of the IR beam with respect to the master clock.

The oscillator consists of Nd:Vanadate crystal, a resonant cavity formed by a saturable absorber mirror (SAM) and an output coupler with 12% transmission. The 4×4×6 mm^3 laser crystal is end-pumped by an 18 W fiber-coupled diode laser operating at 808 nm. The key feature of the oscillator is its repetition rate, too low for conventional CW mode-locking and too high for cavity dumping. To meet the challenge, a folded cavity with a resonator length of 16 m was custom-designed and built. Such a long cavity makes the laser very sensitive to misalignments compared to conventional ~1 m long resonators. To isolate the oscillator from mechanical- and thermal-instabilities, the oscillator is built on a monolithic metal-block and is sealed off from the rest of the system. The SAM is mounted on a stepper motor-driven translational stage with 25 mm travel range to accommodate slow drifts in the cavity length and the coarse tunability of the pulse's repetition rate. Another smaller mirror that is a part of the resonant cavity is mounted on a piezo-driven stage with 9 µm travel range to compensate for fast changes in the cavity length and to preserve synchronization.

The double-pass amplifier consists of a vanadate crystal pumped by a 100 W diode laser operating at 888 nm. The weaker absorption at this wavelength reduces thermal problems, allowing a much higher pump power. The unabsorbed pump power in the first pass is reflected back into the crystal. A Faraday rotator changes the seed beam's polarization from vertical to horizontal after its second pass in the amplifier. The thin film polarizer and the Faraday rotator together inject the seed beam into, and extract it out of the amplifier. The entire pulse train from the oscillator is amplified to eliminate the time-dependent changes in the thermal load induced by the seed- and amplified-pulses. With 100 W pump power, >20 W amplified power at 1064 nm µm was delivered from the amplifier. Figure 13 displays some performance characteristics of the amplified beam.

The pulse selector changes the repetition rate during the ramp-up process for the ERL and also alters its average current without changing the bunch charge. A BBO crystal is used as a Pockels cell, and, the pulses are picked by the polarizing beam-splitter cube (PBS) when the voltage is applied to the crystal, rather than when it is turned off. The BBO can handle the constant high voltage and can be oriented for the best contrast. The high voltage is triggered externally to deliver pulses from single shot to a micro pulse-macro pulse configuration with variable number of micro pulses within a macro pulse, and macro pulse repetition rate variable up to 10 kHz. The entire 9.38 MHz train also can be delivered to the cathode. Some possible configurations are illustrated in Figure 14.

The fundamental 1064 nm radiation is converted into 532 nm and 355 nm by a harmonic crystal for each conversion. The second harmonic crystal is a non-critically phase-matched LBO crystal maintained at 150 C. A vertically polarized beam at 1064 nm, focused to a beam waist of ~300 µm, is converted, with 50% efficiency, to horizontally polarized, 532 nm radiation.

The third harmonic crystal is a non-critically phase-matched LBO crystal maintained at 40 C. The vertically polarized 1064 nm and horizontally polarized 532 nm radiation, focused down to a beam waist of 300 µm, deliver vertically polarized 355 nm beam with power levels of ~5 W. Since the spot size in the crystal is very small and the average- and peak-powers are high, there is a very high probability for surface damage and UV-induced surface degradation. The UV module is purged constantly with hydrocarbon-free air to increase the lifespan of the optical components and coatings. The pointing stability of the beam was measured to be ~3 µrad over 2 hours, well within the range required for the application. The walk-off in the THG crystal causes the appearance of a halo in the transverse profile of the laser beam that must be filtered before it irradiates the cathode.

ISBN 978-3-95450-145-8

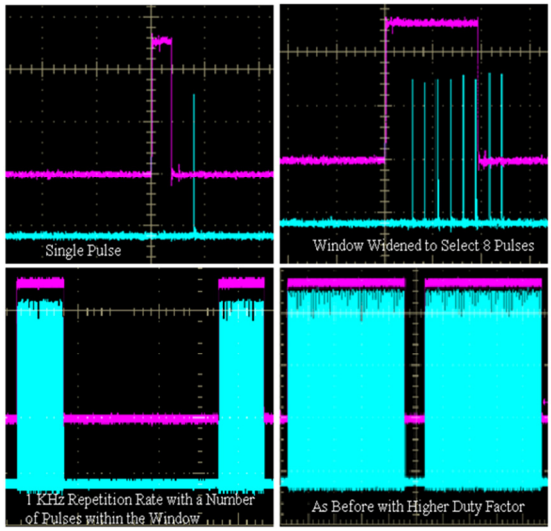

Figure 14: Different configurations of pulses from the pulse picker: Single micro pulse, multiple micro pulses, 1 KHz macro pulse with varying number of micro pulses within the macro pulse envelop. Magenta lines indicate the shape of the high voltage pulse.

The temporal profile of the 532 nm beam is shaped to nearly flat top profile using a stack of three birefringent crystals with lengths of 6, 12 and 24 mm. The conversion of spatial profile to a flat top is accomplished with a commercial shaper. The combined beam has been imaged onto the cathode located at ~9 m from the laser with minimal modification of the profile. The spatial and temporal profiles at different locations from the laser, along with long/short term stability of the system are shown in Figure 15 [38].

Another example laser system for an ERL injector is the fiber laser at Cornell University. The parameters are quite different than the Brookhaven laser described above. For this injector, the operating frequency is 1300 MHz, the same as the RF system, as it is a true CW machine with each RF bucket filled with electrons. The laser must provide enough power to generate 77 pC per bunch at 1300 MHz, or 100 mA average power. For the worst case of a 1% QE cathode, ~20 Watts at 520 nm delivered to the cathode is required. A pulse width of 1-2 ps FWHM is desired, which is then used to make a flat-top pulse in time with a series of birefringent crystals. A jitter of < 1 ps is needed for stable injector operations.

A commercial optical clock (Pritel, Inc) is used as an oscillator to produce 8 ps rms chirped pulses. The output is synchronized to the RF master clock. The power is boosted in two preamplifier sections and one main amplifier, and then de-chirped to make the desired pulse length (Figure 16). The maximum power obtained is 110 Watts IR after de-chirping (with 220 Watts of pump power), and 65 Watts at 520 nm after passing through a second-harmonic generation crystal. The details of this laser are described in [39].

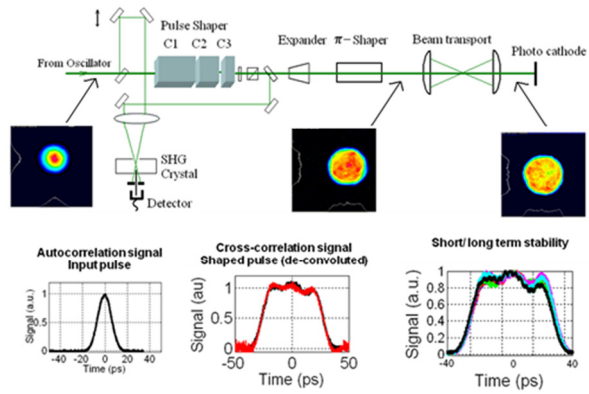

Figure 15: Spatial- and temporal-profile of the laser beam as it propagates along the beam transport. Left: Output of the laser; Middle: Spatially shaped by beam shaper and temporally shaped by beam stacker near the laser; Right: Shaped beam after relay imaging to the cathode location, 9 m away from the laser.

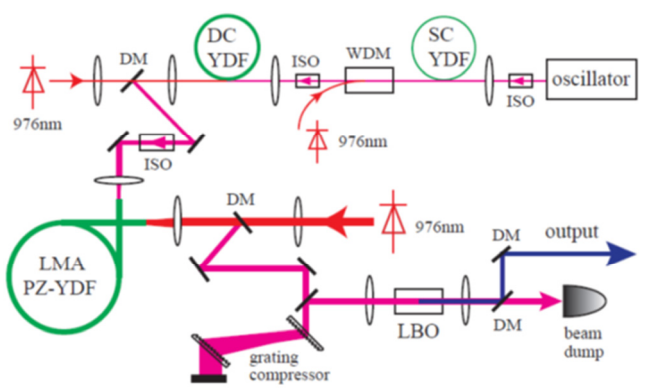

Figure 16: Schematic of the experimental setup: LMA, large mode area; PZ-YDF, single-polarization Yb-doped fiber; WDM, wavelength division multiplexer; SC, single-clad; DC, double-clad; ISO, optical isolator; DM, dichroic mirror.

OPERATIONAL ISSUES

Bruce Dunham

As more and more guns and injectors come on-line, operational issues are increasingly important to consider. This is an indication that intermediate bunch charge, high average power injectors comprised of DC photoemission guns coupled to RF boosters are becoming an accepted solution for many accelerators. In this section, a number of the operational issues encountered during machine commissioning at various labs will be discussed.

Beam halo in an injector is typically produced by different mechanisms than in the main accelerator. There are a number of sources of halo in an injector: field emission from HV electrodes; scattered light from the laser hitting the cathode outside the desired area; light between the main laser pulses (extinction ratio); and x-

ISBN 978-3-95450-145-8

rays/UV or visible light reaching the cathode from many different sources.

To reduce the effects of stray light producing electrons outside the desired cathode area, most groups now use techniques to keep the photo-emissive area as small as possible [40] (see Figure 17). This will definitely reduce halo due to stray light, but will also reduce the active area available for producing a beam after the previously used area decays.

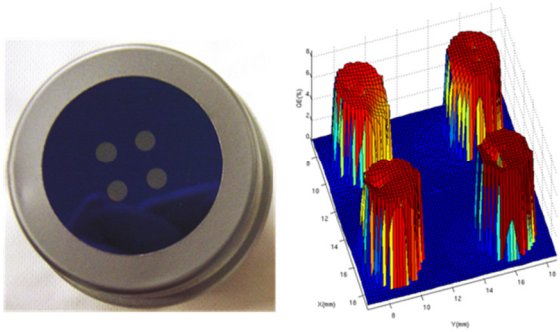

Figure 17: (left) A GaAs cathode is anodized over its entire surface to prevent emission (blue color), then stripped away to expose the clean surface (4 small, gray circles). The right picture shows a QE map of the cathode after use. For best results regarding halo, only one spot would be stripped clean on the left photo.

If a vacuum mirror is used to deflect the laser beam onto the cathode, the quality of the mirror is of critical importance. A mirror surface roughness of < 2 nm-rms is required to keep the fraction of scattered light below 10^{-5} to 10^{-6}. It is not advisable to use dielectric mirrors as they can charge up from any scattered electrons that hit them, but one can purchase commercial mirrors on metal substrates with this surface finish (or better), or use silicon as a substrate.

For the injectors needed for ERLs and FELs, finding diagnostics to handle the huge dynamic range is a challenge. For example, at the high end we care about 100 mA currents, and at the low end maybe as little as 100 pA (for halo and beam loss), which is a dynamic range of 10^9! Some possibilities were discussed in working group 4 of this conference. One simple device is to use a fluorescent view screen with a hole in it: the main beam passes through the central hole while the halo is intercepted on the view screen (see Figure 18).

Feedback systems for high average power machines are important to reduce any transients generated by the beam, especially in the RF cavities. At the Cornell injector, we initially had difficulty exceeding 10 mA average current, as the RF cavities would trip off for currents great than this. This was caused by fast current transients that the RF controls could not correct for. The problem was traced to position jitter in the laser: as the laser passed through a small pinhole for transverse shaping, the position jitter was translated into power fluctuations after the pinhole. A digital fast-feedback system was used to correct for the fluctuations [41] (see Figure 19). The necessary hooks for feedback should be included at an early stage in the injector design.

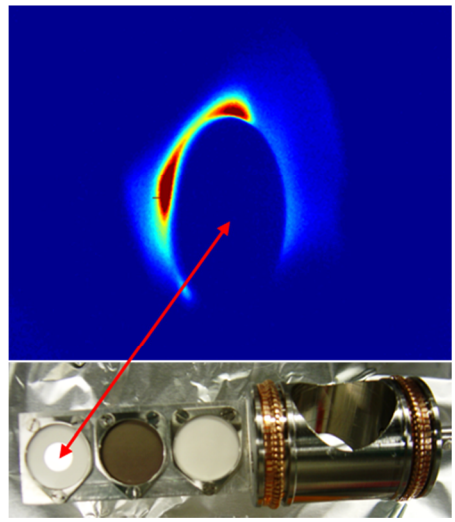

Figure 18: The lower photo shows a multiple viewscreen mechanism, where the left-most fluorescent screen has a 10 mm clear hole through it. The top picture shows halo hitting the edges of the viewscreen while the main beam passes un-impeded through the center.

These are a few examples of operational issues to consider during high average current operations.

FUTURE NEEDS

We discussed various topics that need further research before the next ERL workshop, and list them here.

- GaN-like photocathodes, which may be more robust against vacuum excursions.
- Laser pulse pickers for GHz rep rate lasers, and how to ramp up the beam current for these systems.
- Pockels cells that can handle high average powers (>100 Watts IR)
- Suppliers of optical coatings with high damage thresholds
- Continued work on pushing for higher gun voltages, inverted, segmented or otherwise
- Investigate using GaN diodes for blue light, where cathode QE's are higher
- Continued investigation of high voltage processing using noble gases
- Air core fibers for beam transport and for longitudinal shaping
- Methods for cooling cathodes during high power operation
- Recipe standardization for alkali cathodes
- Improved sources for alkali deposition
- Better diagnostics for halo and beam loss
- Wide dynamic range BPMs and CCD cameras
- Vacuum gauges with a fast response time (< 1ms)
- Easy to use fast DAQ and transient detection
- Fast, high dynamic range photodiodes to look between laser pulses for background light.

ISBN 978-3-95450-145-8

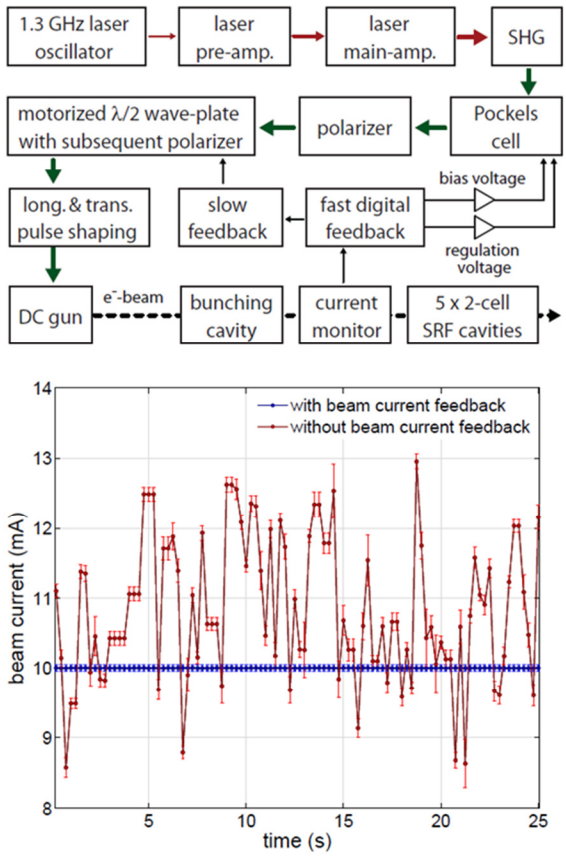

Figure 19: The top shows a block diagram of the digital fast feedback system. The bottom shows the beam current with and without feedback.

CONCLUSIONS

DC photocathode guns have been in existence for several decades now, so it is exciting to see continued improvements over the past several years. Many in the accelerator community do not see DC guns as being very sexy, but these systems are now producing beam with parameters that were thought to be impossible only a few years ago. Thus, they are becoming the electron source of choice for intermediate range bunch charge machines with high average power and high brightness requirements.

ACKNOWLEDGMENTS

The authors would like to thank the organizing committee and all of the contributors to the working group 1 presentation and discussion sessions.

Financial support for the JLab FEL electron gun was provided by the Office of Naval Research, the Army Night Vision Laboratory, the Air Force Research Laboratory, the Joint Technology Office, the Commonwealth of Virginia, and by the U.S. DOE Basic Energy Sciences under Contract No. DE-AC05-060R23177. CEBAF work supported by the U.S. DOE under contract No. DE-AC05-84ER40150.

The CEBAF work is sponsored by Jefferson Science Associates under U.S. DOE Contract No. DEAC05-06OR23177 and with funding from the DOE Office of High Energy Physics and the Americas Region ILC R&D program.

The JAEA work is supported by MEXT Quantum Beam Technology Program.

The Cornell work is sponsored by the National Science Foundation, Division of Materials Research grant number DMR-0807731.

Work at BNL is supported by DoE under Contract No. DE-AC02-98CH10886 with the U.S. DOE.

REFERENCES

[1] N. Nishimori, I. Bazarov, B. Dunham, J. Grames, C. Hernandez-Garcia, L. Jones, B. Militsyn, M. Poelker, K. Surles-Law, and M. Yamamoto, "ERL09 WG1 Summary: DC Gun Technological Challenges," Proceedings of ERL09, Ithaca, NY, pp. 6-23 (2009).

[2] I. Bazarov, L. Cultrera, A. Bartnik, B. Dunham, S. Karkare, Y. Li, X. Liu, J. Maxson and W. Roussel, "Thermal emittance measurements of a cesium potassium antimonide photocathode," Appl. Phys. Lett. **98**, 224101 (2011).

[3] L. Cultrera, I. Bazarov, A. Bartnik, B. Dunham, S. Karkare, R. Merluzzi and M. Nichols, "Thermal emittance and response time of a cesium antimonide photocathode," Appl. Phys. Lett. **99**, 152110 (2011).

[4] D.H. Dowell, I. Bazarov, B. Dunham, K. Harkay, C. Hernandez-Garcia, R. Legg, H. Padmore, T. Rao, J. Smedley and W. Wan, "Cathode R&D for future light sources," Nucl. Instr. Meth. A **622**, 685-697 (2010).

[5] I. Bazarov, et al., "Multivariate optimization of a High Brightness DC Gun Photoinjector," Phys. Rev. ST Accel. Beams **8**, 034202 (2005).

[6] personal communication, B. Dunham.

[7] C. Hernandez-Garcia, T. Siggins, S. Benson, D. Bullard, H. F. Dylla, K. Jordan, C. Murray, G. R. Neil, M. Shinn, and R. Walker, "A High Average Current DC GaAs Photocathode Gun for ERLs and FELs", PAC05, Knoxville, Tennessee, 2005, p. 3117.

[8] I. Bazarov, B. Dunham, Y. Li, X. Liu, D. Ouzounov, C. Sinclair, F. Hannon and T. Miyajima, "Thermal emittance and response time measurements of negative electron affinity photocathodes," J. Appl. Phys. **103**, 054901 (2008).

[9] B. Dunham, L. Cardman and C. Sinclair, Proceedings of the 1995 Particle Accelerator Conference, Dallas, TX, pg. 1030 (1995).

[10] D. H. Dowell et al., Appl. Phys. Lett. **63**, 2035 (1993).

[11] T. Vecchione, I. Ben-Zvi, D. Dowell, J. Feng, T. Rao, J. Smedley, W. Wan, H. Padmore, "A low emittance and high efficiency visible light photocathode for high brightness accelerator-based X-ray light sources," Appl. Phys. Lett. **99**, 034103 (2011).

[12] J. Grames, R. Suleiman, P. Adderley, J. Clark, J. Hansknecht, D. Machie, M. Poelker, and M. Stutzman, "Charge and fluence measurements of a dc

ISBN 978-3-95450-145-8

high voltage GaAs photogun at high average current," Phys. Rev. ST Accel. Beams 14, 043501 (2011).
[13] L. Cultrera, J. Maxson, I. Bazarov, S. Belomestnykh, J. Dobbins, B. Dunham, S. Karkare, et al., "Photocathode behaviour during high current running in the Cornell energy recovery linac photoinjector," Phys. Rev. ST Accel. Beams **14**, 120101 (2011).
[14] I. Bazarov, B. Dunham, X. Liu, M. Virgo, A. Dabiran, F. Hannon and H. Sayed, "Thermal emittance and response time measurements of a GaN photocathode," J. Appl. Phys. **105**, 083715 (2009).
[15] Charles K. Sinclair, "DC photoemission electron guns as ERL sources," Nucl. Inst. and Meth. A **557** (2006) 69.
[16] C.W. de Jager, V. Y. Korchagin, B.L. Militsyn, V.N. Osipov, N.H. Papadakis, S.G. Popov, M.J.J. van den Putte, Yu. M. Shatunov, Yu. F. Tokarev, "The Photocathode Gun of The Polarized Electron Source at NIKHEF," The Seventh International Workshop on Polarized Gas Targets and Polarized Beams, AIP Conf. Proc. 421 (AIP, New York, 1998), 483.
[17] Tsutomu Nakanishi, "Polarized electron source using NEA-GaAs photocathode", Proc. of LINAC2002, Gyeongju, Korea, 811.
[18] N. Nishimori, R. Nagai, R. Hajima, T. Shizuma, E.J. Minehara, "A Thermionic Electron Gun System for the JAERI Superconducting FEL," Proc. of EPAC00, Vienna, Austria, 2000, 1672.
[19] N. Nishimori, R. Nagai, H. Iijima, Y. Honda, T. Muto, M. Kuriki, M. Yamamoto, S. Okumi, T. Nakanishi, and R. Hajima, "Development of an electron gun for an ERL based light source in Japan," Proceedings of the 18th International Symposium on High Energy Spin Physics (SPIN2008), (Ref. [6]), 1094.
[20] P.G. Slade, "The vacuum interrupter: theory, design, and application," CRC Press, 2008.
[21] R. Nagai, R. Hajima, N. Nishimori, T. Muto, M. Yamamoto, Y. Honda, T. Miyajima, H. Iijima, M. Kuriki, M. Kuwahara, S. Okumi, and T. Nakanishi, "High-voltage testing of a 500-kV dc photocathode electron gun," Rev. Sci. Instrum. **81**, 033304 (2010).
[22] B. Dunham, private communication.
[23] M. Yamamoto, private communication.
[24] Jiuqing Wang, private communication.
[25] P. Massmann, H.P.L. de Esch, R.S. Hemsworth, T. Inoue, and L. Svensson, "The Cadarache 1 MV porcelain SINGAP bushing," Fusion Eng. Des. **56-57**, (2001) 539-544.
[26] L. Svensson, D. Boilson, H.P.L. de Esch, R.S. Hemsworth, A. Krylov, and P. Massmann, "Latest results from the Cadarache 1 MV SINGAP experiment," Fusion Eng. Des. **66-68** (2003) 627-631.
[27] A. Masiello, "Adaption of the 1MV bushing to the SINGAP concept for the ITER NB injector test bed," Nucl. Fusion **46** (2006) S340-S351.
[28] P. Adderley, J. Clark, J. Grames et al., Phys. Rev. ST Accel Beams **13**, 010101 (2010).
[29] P. A. Adderley, J. Clark, J. Grames, et al., "CEBAF 200 kV Inverted Electron Gun," Proceedings of the 2011 Particle Accelerator Conference, New York, NY. WEBODS3.
[30] B. M. Dunham and K. W. Smolenski, "Voltage DC photoemission electron gun at Cornell University," Power Modluator and High Voltage Conference, 2010 IEEE International, Atlanta GA, 23-27 May 2010.
[31] C. Hernandez-Garcia, S. Benson, G. Biallas, D. Bullard, P. Evtushenko, K. Jordan, M. Klopf, D. Sexton, C. Tennant, R. Walker, and G. Williams, "DC High Voltage Conditioning of Photoemission Guns at Jefferson Lab FEL," Proceedings of the 18th International Symposium on High Energy Spin Physics (SPIN08), edited by D. Crabb, D. B. Day, S. Liuti, X. Zheng, M. Poelker and Y. Prok. 2009 AIP, p. 1071.
[32] N. Nishimori, R. Nagai, H. Iijima, Y. Honda, T. Muto, M. Kuriki, M. Yamamoto, S. Okumi, T. Nakanishi, and R. Hajima, "Status of 500-kV DC gun at JAEA," presented at ERL11, KEK, Japan, 2011.
[33] M. BastaniNejad, P. Adderley, J. Clark, et al., "Field Emission measurements from Niobium Electrodes," Proceedings of the 2011 Particle Accelerator Conference, New York, NY. WEB287.
[34] P. Kneisel, "Cavity Preparation and Assembly Techniques and Impact on Q, Realistic Q-factors in a Module, Review of Modules," Proceedings of the ERL05 Workshop.
[35] M. Yamamoto et al., Proc. International Particle Accelerator Conference (IPAC2011), San Sebastian, Spain, p.979.
[36] H. Yamakawa, Vacuum **44**, (1993) 675.
[37] H. Yoshida et al., "New leak element using sintered stainless steel filter for in-situ calibration of ionization gauges and quadrupole mass spectrometers," Vacuum (2011), doi:10.1016/j.vacuum.2011.02.013 [in press].
[38] A.K. Sharma, T. Tsang, and T. Rao, "Theoretical and Experimental Study of Passive Spatio-Temporal Shaping of Picosecond Laser Pulses," Phys. Rev. Special Topics **12**, 033501 (2009).
[39] Z. Zhao, in press.
[40] C.K. Sinclair, P. Adderley, B. Dunham, J. Hansknecht, P. Hartmann, M. Poelker, J. Price, P. Rutt, W. Schneider and M. Steigerwald, "Development of a high average current polarized electron source with long cathode operational lifetime," Phys. Rev. ST Accel. Beams 10, 023501 (2007).
[41] F. Loehl and P. Szypryt, "Active Beam Current Stabilization in the Cornell ERL Prototype Injector," Proceedings of the International Particle Accelerator Conference 2011, San Sebastian, Spain, pp. 523-525.

ISBN 978-3-95450-145-8

ERL2011 SUMMARY OF WORKING GROUP 1: PROGRESS WITH RF INJECTORS

T. Rao[1], A. Arnold[2], S. Belomestnykh[1], D. Nguyen[3], T. Quast[4]
[1]Brookhaven National Laboratory, Upton, NY 11973 USA
[2]Helmholtz-Zentrum Dresden-Rossendorf, Germany
[3]Los Alamos National Laboratory, Los Alamos, NM 87545 USA
[4]Helmholtz-Zentrum Berlin, Germany

Abstract

This paper summarizes the progress made in the past two years with RF injectors as electron sources for high average power Energy Recovery Linacs (ERL).

INTRODUCTION

Many ERL applications call for lowest emittance and highest brightness from electron injectors. The inherent capability of RF injectors to support high cathode field gradients makes them ideally suited for high bunch charge, low emittance applications. However, the price to be paid for the high gradient and high average current is the associated high thermal load and its management. Two different approaches have been adopted for thermal management: use of superconducting cavities that have inherently lower thermal load versus incorporation of elaborate cooling channels in normal conducting cavities. In the last two years there has been considerable progress towards the development of normal conducting RF (NCRF) and superconducting RF (SRF) guns to meet these challenges. Two additional major considerations in designing the gun are the RF power coupling and integration of the cathode in the gun. In this paper, we will discuss the latter topics and cover the latest developments with the NCRF and SRF guns.

FUNDAMENTAL POWER COUPLERS FOR SRF GUNS

SRF electron guns based on elliptical cavities use traditional way of coupling RF power to SRF cavities via coaxial antennae connected to beam pipe ports. At lower RF power a single fundamental power coupler (FPC) is used [1, 2], while at high power two FPCs, symmetrically placed, are used to lower power load per coupler and eliminate transverse kick for beam on axis [3]. The latter FPCs (Fig. 1) were successfully tested in standing wave regime with full reflection up to 250 kW in pulsed mode and 125 kW in CW mode [4].

An alternative to the elliptical cavity design is the coaxial quarter-wave resonator (QWR) design. It has an advantage of smaller dimensions compared to elliptical cavities for the same frequency, or given the same size, the quarter-wave design operates at a lower frequency. QWR guns designed so far will operate with low average beam currents and hence low RF power. Due to the gun geometry and low frequency, the FPC design of choice is based on a coaxial beam tube at the beam exit [3, 5-6]. These couplers (Fig. 2) are axially symmetric and, if properly designed, should cause even less beam disturbance than two antenna-type couplers.

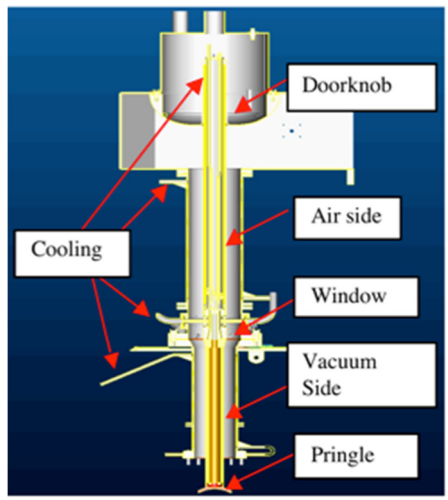

Figure 1: Coaxial antenna-type FPC for ½-cell elliptical cavity SRF gun at BNL [4].

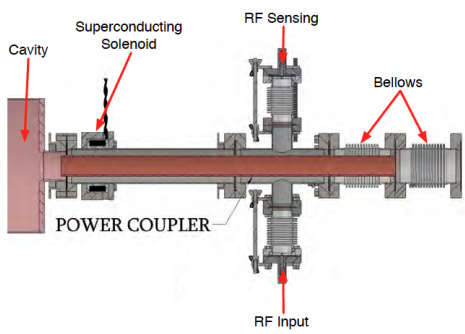

Figure 2: Coaxial beam line FPC for the quarter-wave resonator SRF gun at NPS [7].

PHOTOCATHODE SELECTION AND INTEGRATION

The photocathodes for the high current operation has to meet a number of special requirements: they need to have quantum efficiency (QE) in the range of a few percent at a wavelength where high power lasers are readily available. In addition, they must be robust, prompt in electron emission, should have very high surface charge limit and insensitive to vacuum incursion that may occur in an

ISBN 978-3-95450-145-8

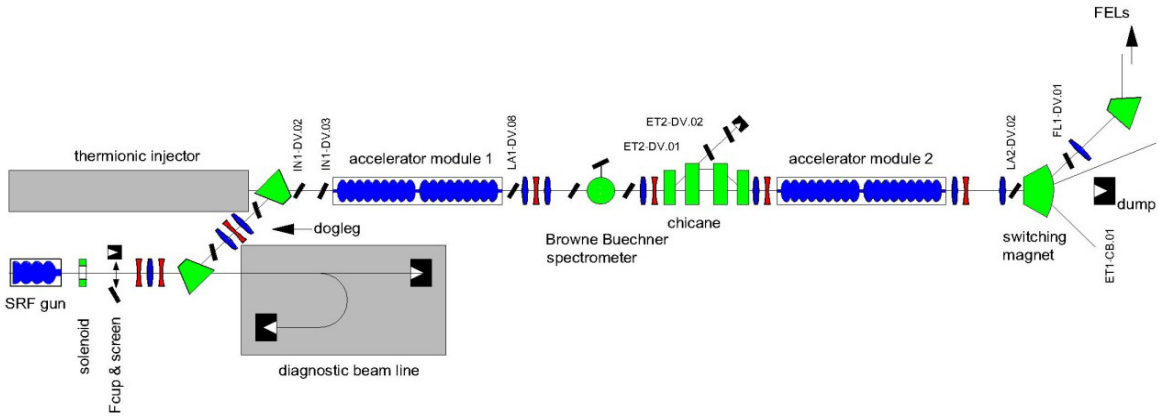

Figure 3: Beamline layout of the SRF gun, dogleg section, and ELBE linac.

operating gun environment. In a number of gun designs, it is preferable to characterize the gun at low average currents prior to operating it in its full capability. Different commissioning stages can then be decoupled from each other and the subsystems can be tested independently with minimal complications. As evidenced in the B*ERL*inPro approach below, this characterization can be accomplished with a metal photocathode, which can later be replaced by a high QE one.

Incorporating the photocathode into the RF gun is still an evolving field, especially when a normal conducting cathode is used in a SRF injector. For average currents << 1 mA, metal photocathodes are still a viable option. In such a case, a cathode (for example, a superconducting cathode such as lead) can be deposited onto the back wall of the cavity. For higher average currents, high QE cathodes need to be used. If the cathode life time is not long enough, care must be taken in the engineering of the cathode insertion so that the cavity stays superconducting while the spent cathode is being exchanged for a fresh one. One of the designs is described in [8]. In this, a batch of cathodes is prepared ex-situ in an ultra-high vacuum (UHV) chamber and is transported to an exchange chamber which is attached to the cryostat via an UHV transfer chamber. A cathode is then moved from the exchange chamber to the gun cavity by a transfer rod. An additional concern is the effective transport of the emitted electrons from the cathode to the booster cavity. Matching the beam radius to the booster cavity's gradient and exit energy must be done appropriately to minimize emittance growth.

Similar load-lock approach has been applied to NCRF injectors also, without the added complication of maintaining the cavity at superconducting temperatures.

STATUS OF INJECTORS

Rossendorf SRF Gun: Operational Experience

The SRF gun for the superconducting linear accelerator ELBE was developed within a collaboration of the German institutes BESSY/HZB, DESY, MBI and HZDR and put into operation in 2007. Details of the design have been published in [8]. During the first two years of operation a lot of experience was gained using a separate diagnostic beamline [9]. Most of the results have been published in the summary paper of working group 1 of the 2009 ERL workshop [10].

Since 2010, the SRF gun is connected to the ELBE accelerator. The corresponding beam line layout is presented in Fig. 3. It consists of a solenoid for emittance compensation, followed by a screen station, a movable Faraday cup and a quadrupole triplet. The connecting dogleg is arranged about 1.5 m in front of the SRF gun exit using a 45° dipole magnet, which deflects the beam towards the ELBE linac, followed by a quadrupole triplet and ends with a second 45° magnet in front of the first acceleration module of ELBE. A photograph of the installation is shown in Fig. 4. Although the realized beam injection scheme with the dispersive part in the dogleg is disadvantageous since the gun produces high correlated energy spread, it can be compensated in the first acceleration module after the dogleg.

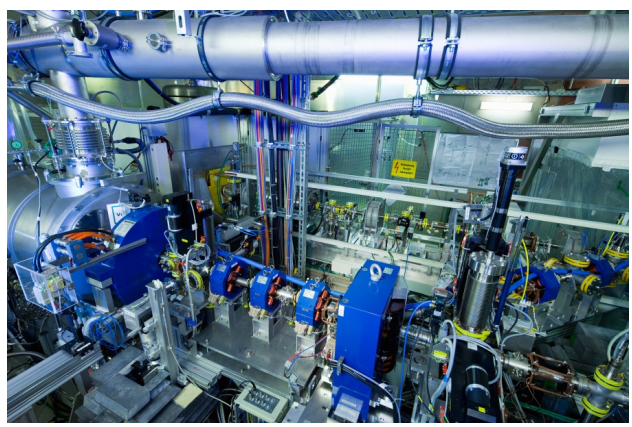

Figure 4: Photograph of the SRF gun with the beamline and dogleg.

The standard gun operation is continuous wave (CW). But to reduce the heat load and operate at higher gradient, the input RF is temporarily pulsed with repetition rate of 1 to 10 Hz, and the pulse length adjustable between 5 and 20 ms. Typical fields and gradients for both operations are listed in Table 1. In this mode the gun delivers an electron beam with the kinetic energy of 3 MeV,

ISBN 978-3-95450-145-8

accelerated by the peak electric field of 16.5 MV/m. Due to the lower field in the half-cell, the retracted photo cathode and the early launch phase with respect to the RF crest value (90°), the field at electron bunch emission is rather low (see Table 1).

In both CW and pulsed cases, a bias voltage of -5 kV is usually applied to the cathode. Although defocusing, this additional voltage increases the field at the cathode and improves slightly the beam quality.

Up to now, the maximum bunch charge injected and accelerated in ELBE is 120 pC, with a pulse repetition rate of 50 kHz (6 μA). Energy spread of the beam has been measured in the ELBE beam line using Brown Buechner spectrometer. For CW operation with 6 MV/m accekerating gradient and 10 pC bunch charge, the energy spread is the lowest, ~ 20 keV at a launch phase between 0° and 10°, as shown in Fig. 5. The longitudinal phase space ellipse has been measured in CW and pulsed mode with beam energies of 3.0, 3.5, 4.0 MeV and bunch charges between 10 and 100 pC. More details of the method are described elsewhere [11, 12]. The electron bunch length has been measured as a function of the launch phase for 4 MeV beam energy and 10, 50 and 100 pC bunch charges. For optimum launch phase, the electron bunch lengths were approximately one half of the laser pulse duration of 6 ps.

Table 1: Typical Parameters of the HZDR SRF Gun for CW and Pulsed Mode

Gun operation mode	CW	Pulsed RF
Accelerating gradient	6 MV/m	8 MV/m
Electron kinetic energy	3 MeV	4 MeV
Peak field on axis	16.5 MV/m	21.5 MV/m
Peak field at the cathode (2.5 mm retracted)	6.5 MV/m	8.4 MV/m
Cathode field at launch phase (10°)	1.1 MV/m	1.5 MV/m
Cathode field at 10° and -5 kV bias	2.2 MV/m	2.6 MV/m

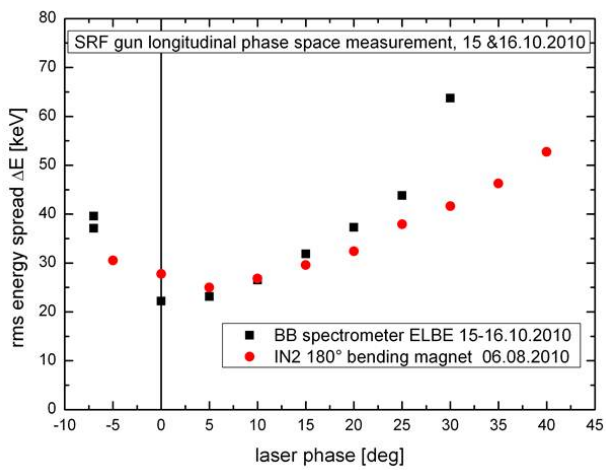

Figure 5: Energy spread measurements for 3 MeV and a bunch charge of 10 pC, using the Brown Buechner spectrometer in ELBE and the 180° bending magnet in the diagnostics beamline.

Cavity Performance

The Q of the cavity was measured in vertical tests as well as in the beam line, with and without the cathode inserted in the cavity. Although the intrinsic quality factor of $Q_0 \approx 3 \cdot 10^9$ in the beam line is ten times lower than that in all vertical tests, the RF performance of the cavity did not change with the insertion of the cathode. It is assumed that contamination during clean room assembly is the most likely reason for the performance degradation between vertical tests and in the beam line.

Using the frequency shift during cool down, the coefficient of thermal expansion and the total change of the cavity length of $\alpha_{20} = +6.8 \cdot 10^{-6}\ \mathrm{K}^{-1}$ and $\Delta l/l = -0.155\%$ were established. The field distribution at a cryogenic temperature was calculated using algorithm published in [13] and found to be (-62% / 99.4% / -97.5% / 100%) starting in the half-cell, well within design parameters. The static helium and liquid nitrogen heat loads were measured to be ≈ 7 W and ≈ 32 W respectively, both within the specifications.

The frequency sensitivity with respect to helium pressure fluctuations was found to be ~150 Hz/mbar, which is five times the value known for TESLA cavities. Nevertheless, this is not critical for operation due to the good helium pressure stability of ~ 0.1 mbar and cavity bandwidth of ~ 160 Hz. Since the Lorentz detuning was measured to be three times larger than known from TESLA cells due to the weak half-cell, an additional stiffener is used in the upgrade cavities [14].

Another important property of the cavity is its frequency detuning due to mechanical vibrations, known as microphonics. There are three main contributors: the helium refrigerator, the membrane pumps and the first mechanical cavity eigenmode. The residual phase error of $\sigma_\varphi = 0.05°$ is more than sufficient for ELBE operation and does not depend on the gradient. The frequency error is calculated to be $\sigma_f = -BW/2 \cdot \tan(K_p \cdot \sigma_\varphi) \approx 6$ Hz, which is typical for TESLA cavities operated at ELBE. The typical closed loop gain and bandwidth during operation are $K_p = 100$ and $BW = 150$ Hz, respectively.

Finally, the cavity tuners have been characterized. Because of different mechanical properties, there is one tuner for the half-cell and another one for the TESLA cells. The tuner for the half cell has an excellent resolution of 0.3 Hz/step combined with a negligible hysteresis and a tuning range of ±78 Hz. The second tuner is slightly worse but, because of its higher tuning range of ±225 kHz, still good enough for rough cavity tuning.

Photocathodes

Since 2005 the photocathode laboratory has been in operation at HZDR. The main goal is to prepare Cs_2Te photocathodes for the SRF gun. At the same time activities are directed towards new photocathode

ISBN 978-3-95450-145-8

materials with high QE for high current electron sources. A vacuum transport system with UHV is used to move the cathodes from the preparation lab to accelerator hall. Up to now, 31 Cs_2Te photocathodes have been deposited and eight of them have been used in the SRF gun. The quantum efficiency of 1% and life time of months can be maintained during the gun operation.

Based on simulations, multipacting (MP) is expected in the gap between the cathode hole of the cavity and the cathode plug at the location of 5.5 mm behind the cathode surface. Negative cathode bias up to 5 kV is designed to prevent MP, which is efficient in most cases. A structure with multi rings on the cathode plug has been developed to minimize the risk of MP in this gap. However, cesium contamination of the cathode in the sensitive area, during deposition process could exacerbate the multipacting. This explanation is supported by the measurements that shows 30% increase in the field emission current from Mo/CsTe cathodes compared to bare metal cathodes as seen in Fig. 6.

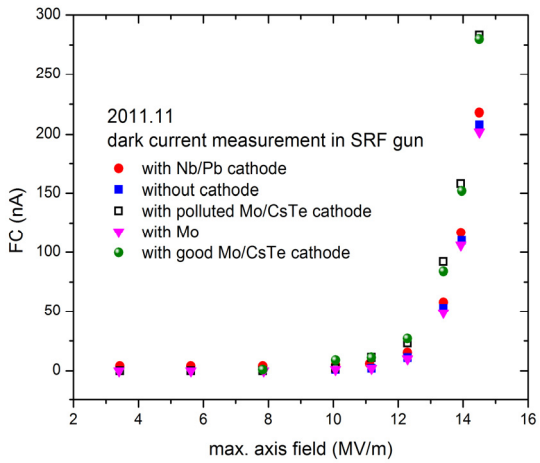

Figure 6: Dark current measured in the Faraday cup downstream of the gun versus maximum axis field. The blue squares show the cavity without a cathode. Four different cathodes have been measured in this experiment.

BERLinPro SRF Gun at HZB

The final goal of the SRF injector at the B*ERL*inPro is to deliver 100 mA current with repetition rate of 1.3 GHz and the emittance goal of 1mm·mrad at 1.5 MeV. In order to achieve this goal, a three-stage approach has been adapted. In the first phase, the focus is on the beam

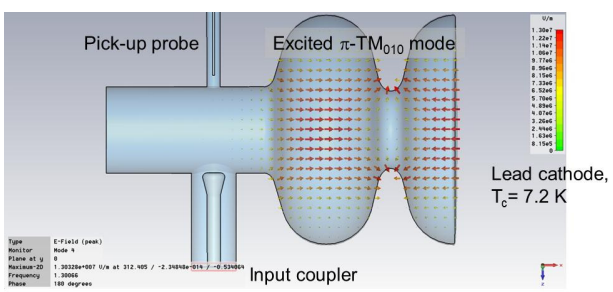

Figure 7: Schematic of the 1½-cell, 1.3 GHz SRF gun.

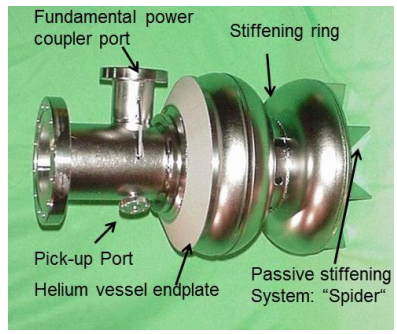

Figure 8: Photograph of the B*ERL*inPro Stage 1 SRF gun.

dynamics of the SRF injector, with emphasis on RF performance and beam stability. The schematic design and a photograph of the 1½ cell SRF gun, designed by J. Sekutowicz, DESY, are shown in Fig. 7 and 8 respectively.

Studies of field stability indicate that stiffening of the back plate of the cavity with a "spider" shaped support reduces the deformation to < 2 μm from > 8 μm for the unsupported cavity, resulting in reduced sensitivity to the fluctuations in He pressure. The Q_0 of this cavity prior to the cathode deposition, measured in a vertical test facility, was greater than 1×10^{10} for peak E fields < 35 MV/m.

A lead cathode was deposited on to the central 5 mm of the cavity back wall using a plasma arc deposition set up with the cathode positioned at 30° to the source to minimize deposition of large droplets on the cathode as shown in Fig. 9. Both Q_0 and the threshold for field emission were reduced after Pb deposition. However, laser cleaning of the cathode, a necessary step to remove the adsorbed impurities, restored the field emission threshold from 12 MV/m at HoBiCaT to 18 MV/m.

The first photoemission beam of 50 nA current, 3-4 ps bunch length and 5-6 pC bunch charge was observed when the laser-cleaned cathode was irradiated with 258 nm laser beam [16]. The maximum electron energy, based on the dipole scan and simulations has been estimated to be ~1.8 MV. Work is underway to measure the intrinsic and beam emittances and to improve the cavity parameters.

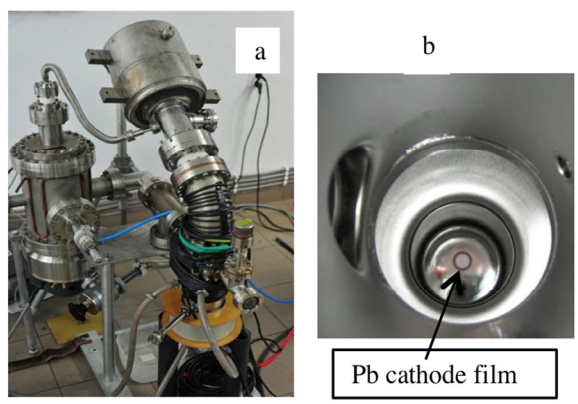

Figure 9: Photographs of the plasma arc deposition system (a) and Pb cathode film (b). The deposition was done by R. Nietubyc at NCBS.

ISBN 978-3-95450-145-8

SRF Guns at BNL

Two SRF guns are under development at BNL [17]. The ½-cell elliptical cavity gun belongs to the first generation of SRF guns. It was designed and fabricated by AES. The gun operates at 703.75 MHz and with the goal to produce high average current (up to 500 mA), high bunch charge (up to 5 nC) electron beams for the R&D ERL using K_2CsSb photocathode.

The gun cavity has been tested vertically several times in 2010. The fundamental power couplers (FPCs), manufactured by CPI/Beverly, have been conditioned recently with maximum RF power of 125 kW CW in full standing wave mode [18, 19]. The cavity has been cleaned and the cavity string assembled at JLab. Assembly of the cryomodule is in the progress at BNL (Fig. 10). The first cold test of the gun and subsequent beam generation are scheduled for 2012.

The second gun is a 112 MHz quarter-wave resonator, designed to generate 2 MeV, high bunch charge (>1 nC), low repetition rate (78 kHz) beam for the Coherent electron Cooling (CeC) experiment, as well as for use in photocathodes studies.

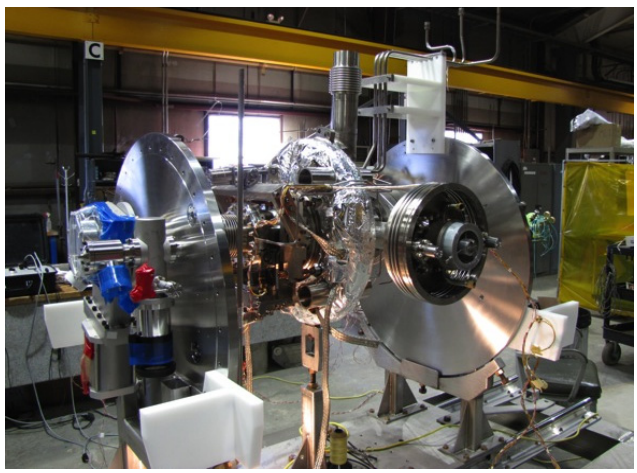

Figure 10: Photograph of the 704 MHz SRF gun cavity string being prepared for assembly into the cryomodule.

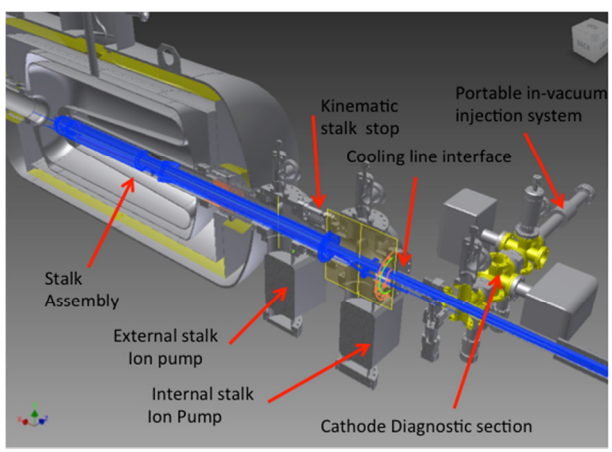

Figure 11: Cathode stalk and load lock system of the 112 MHz QWR electron gun.

The gun was developed by collaborative efforts of BNL and Niowave, Inc. and has been cold tested successfully [20]. It is now being modified for compatibility with the CeC experiment. A low-RF-loss cathode stalk and load lock system for multi-alkali photocathodes is designed (Fig. 11), and its fabrication has started. The gun will be equipped with a combine function FPC/tuner assembly [21]. The design of other upgrades and modifications is in progress.

NCRF Gun at Los Alamos

The continuous-wave normal-conducting RF gun at Los Alamos has produced its first photoelectron beam with a K_2CsSb photocathode driven by a blue laser diode. The NCRF gun has undergone extensive testing with high-power RF to validate its thermal and RF integrity during CW operation. These tests have shown that in addition to heat removal from RF surfaces, the cooling and alignment of critical components such as the RF windows, photocathode plugs have to be properly implemented to ensure successful CW operation of the NCRF gun. K_2CsSb photocathodes with QE on the order of 1% and $1/e$ lifetime of 20 hours are routinely prepared in an UHV deposition chamber. These K_2CsSb photocathodes are then transferred in vacuum to the NCRF gun for testing. The transfer of K_2CsSb photocathodes from the deposition chamber to the gun has to be carefully executed to minimize QE degradation and contamination to the gun that would otherwise increase field emission. Both photocurrent and dark current have been measured using a wall current transformer with typical dark current in the range of 10s of microamperes. Plans are underway to produce picosecond electron bunches at high repetition rates with K_2CsSb photocathodes driven by the green (second harmonic) pulses from a mode-locked Nd:YVO_4 laser in phase with the cavity RF signal.

Other High Current RF Injectors

Beside the injectors mentioned above, there are a number of NCRF and SRF injectors under development.

The Naval Postgraduate School Mark I SRF injector, built by Niowave, Inc. and operated in collaboration with the Boeing Company, produced its first beam in June of 2010 [5]. The Mark I was intended primarily as a research and development tool to explore issues in designing and operating SRF guns in general, and quarter wave SRF guns in particular, although it can serve as an injector for the NPS Beam Physics Laboratory's linac. It uses an on-axis coaxial RF power coupler, and has a resonant frequency of 500 MHz. This low frequency allows operation at 4 K, thereby greatly simplifying the requirements to the cryogenic support system. Nominal beam energy is 1 MeV, with a maximum attained energy of 0.5 MeV to date.

The APEX/VHF NCRF gun [22] operating at 187 MHz has successfully undergone RF conditioning. The gun was run in continuous wave mode and at the nominal power of 100 kW for about 29 hours without faults. The installation

ISBN 978-3-95450-145-8

of the electron beamline with the low energy beam diagnostics is near completion.

University of Wisconsin has built a ~200 MHz SRF injector [23] that is expected to be cold tested in early 2012, with the final assembly scheduled for the summer of 2012 and the first beam anticipated in fall of 2012.

REFERENCES

[1] A. Arnold, "Rossendorf SRF Gun Operational Experience," this workshop.

[2] K. Liu, et al., "DC-SRF photocathode injector for ERL at Peking University," this workshop.

[3] S. Belomestnykh, "Status of BNL SRF guns," this workshop.

[4] S. Belomestnykh and Wencan Xu, "Fundamental power couplers for the ERL prototype SRF gun at BNL," this workshop.

[5] J. Harris, et al., "Design and operation of a superconducting quarter-wave electron gun," *Phys. Rev. ST Accel. Beams* **14** (2011) 053501.

[6] R. Legg, et al., "Development of a Frequency Map for the WiFEL SRF Gun," Proc. SRF'11, 2011, Chicago, IL, to be published, MOPO032.

[7] S. Niles, "Design and Analysis of an Electron Gun/Booster and Free Electron Laser Optical Theory," PhD dissertation, Naval Postgraduate School, Monterey, CA, 2010.

[8] A. Arnold et al., "Development of a superconducting radio frequency photoelectron injector," *Nucl. Instrum. Meth A* **577** (2007) 440-454.

[9] T. Kamps, et al., "Electron beam diagnostics for a superconducting radio frequency photoelectron injector," *Rev. Sci. Instrum.* **79** (2008) 093301.

[10] J. W. Lewellen, et al., "ERL 2009 WG1 Summary Paper: Drive Lasers and RF Gun Operation and Challenges," Proc. ERL'09, 2009, Ithaca, NY, USA, 2009, p. 24-36.

[11] D. H. Dowell, et al., "Longitudinal emittance measurements at the SLAC gun test facility," *Nucl. Instrum. Meth. A* **507** (2003) 331-334.

[12] J. Teichert, et al., "Pulsed Mode Operation and Longitudinal Parameter Measurement of the Rossendorf SRF Gun," Proc. IPAC'11, 2011, San Sebastian, Spain, p. 262.

[13] A. Arnold, et al., "Field Reconstruction by Passband Frequency Measurement at the Rossendorf SRF-Gun Cavity," Proc. SRF'07, 2007, Beijing, China, p. 689-691.

[14] P. Murcek, et al., "Modified 3½-Cell SC Cavity Made of Large Grain Niobium for the FZD SRF Photoinjector," Proc. SRF'09, 2009, Berlin, Germany, p. 585-588.

[15] T. Kamps, et al., "Status and perspectives of superconducting radio-frequency gun development for BERLinPro," J.Phys.Conf. Ser.298:012009, 2011.

[16] T. Kamps, et al., "First Demonstration of Electron Beam Generation and Characterization with an all Superconducting Radiofrequency (SRF) Photoinjector," Proc. IPAC'11, 2011, San Sebastián, THPC109.

[17] S. Belomestnykh, "Status of BNL SRF guns," this workshop.

[18] W. Xu et al., "Conditioning fundamental power couplers for the ERL SRF Gun," Proc. SRF'11, 2011, Chicago, IL, to be published, TUPO010.

[19] S. Belomestnykh and W. Xu, "Fundamental power couplers for the ERL prototype SRF gun at BNL," this workshop.

[20] S. Belomestnykh, et al., "Superconducting 112 MHz QWR Electron gun," Proc. SRF'11, 2011, Chicago, IL, to be published, MOPO054.

[21] T. Xin, et al., "Design of the fundamental power coupler and photocathode inserts for the 112 MHz superconducting electron gun," Proc. SRF'11, 2011, Chicago, IL, to be published, MOPO014.

[22] F. Sannibale, et al., "Status of the LBNL normal-conducting CW VHF electron photo-gun," Proc. FEL'2010, Malmo, Sweden, 2010, p. 475-478.

[23] R. Legg, et al., "SRF photoinjector R&D at University of Wisconsin," Proc. ERL'09, Ithaca, NY, USA, 2009, p. 45-49.

ISBN 978-3-95450-145-8